Research on Engineering Structures & Materials
www.jresm.org
Research Group

Research Article

Statistically validated multi-objective optimization and experimental verification of nanofluid-assisted MQL hard turning of hardened AISI 4140 steels

Huu-That Nguyen [a], Ngoc-Chien Vu [*,b]

Department of Mechanical Engineering, School of Engineering and Technology, Nha Trang University, Nha Trang, Vietnam

Article Info

Article History:

Received 12 Mar 2026

Accepted 28 Aug 2026

Keywords:

Hard turning;
Nanofluid-assisted MQL;
Statistically validated modeling;
Multi-objective optimization;
Surface roughness

Abstract

Hard turning of hardened steels requires simultaneous control of surface integrity, thermal behavior, and productivity, which becomes more challenging under minimum quantity lubrication (MQL) due to its limited cooling capability. Although nanofluid-assisted MQL has demonstrated improved tribological performance, many machining optimization studies rely on surrogate models without rigorous statistical verification, potentially reducing the reliability of the obtained optimal solutions. This study proposes a statistically validated multi-objective optimization framework for hard turning of heat-treated AISI 4140 steel using coconut oil–based MQL enhanced with CuO nanoparticles. A Taguchi L27 experimental design was employed to evaluate the effects of cutting speed, feed rate, and depth of cut on surface roughness (Ra), cutting temperature (Tc), and material removal rate (MRR). Response surface models were systematically validated through analysis of variance, residual diagnostics, multicollinearity assessment, and prediction error analysis before optimization. The results reveal distinct governing mechanisms: Ra is primarily dominated by nonlinear feed effects associated with chip formation kinematics, whereas Tc is mainly controlled by depth of cut due to thermomechanical loading at the tool–chip interface. Multi-objective optimization using NSGA-II generates nominal Pareto trade-offs, and three selected decision regimes are locally confirmed through single-run machining tests. The proposed framework provides a statistically reliable decision-support approach for sustainable hard turning.

© 2026 MIM Research Group. All rights reserved.

1. Introduction

Hard turning of hardened steels is now considered a key enabling process for sustainable manufacturing, as it can replace conventional multi-stage grinding while reducing energy consumption, coolant use, and the overall environmental burden. In industrial practice, heat-treated AISI 4140 steel is widely used in automotive, machinery, and tooling applications because of its high strength and wear resistance; however, machining this difficult-to-cut material remains challenging because of severe tool wear, elevated cutting temperatures, and stringent surface integrity requirements [1-5]. Therefore, achieving an acceptable balance among surface quality, thermal stability, and productivity remains a critical issue for sustainable hard turning.

Minimum quantity lubrication (MQL) has been increasingly adopted as an environmentally benign alternative to flood cooling, because it markedly reduces lubricant consumption while maintaining acceptable machining performance [1, 6-10]. To further improve MQL effectiveness, nanoparticle-enhanced vegetable oils have attracted significant attention in recent years. Numerous studies have

*Corresponding author: chienvn@ntu.edu.vn
[a]orcid.org/0000-0002-6428-2532; [b]orcid.org/0000-0002-4069-2369
DOI: http://dx.doi.org/10.17515/resm2026-1563ma0312rs

reported that the addition of solid nanoparticles, including CuO, Al_2O_3, MoS_2, and graphene-based particles, can improve the thermo-tribological performance of vegetable oils through rolling, mending, polishing, and tribofilm-forming mechanisms, thereby reducing friction and cutting temperature and improving surface finish [4, 11-19]. In this context, it is helpful to distinguish between fluid MQL (base oil only) and nanofluid MQL (nanoparticle-added oil). Particularly, CuO nanoparticles dispersed in biodegradable vegetable oils show promising results, mainly due to high thermal conductivity and favorable interaction at steel tool–workpiece interfaces [14, 20-23].

In parallel with experimental works, surrogate-based modeling and optimization have been widely used to analyze and optimize machining responses under MQL conditions [5, 11, 12, 14, 24-28]. Typically, DOE is used to generate experimental data. Then RSM is used to build empirical relationships between cutting parameters and key responses, such as surface roughness, cutting temperature, and material removal rate [3, 5, 11, 12, 24-31]. Kriging or Gaussian process regression has also been utilized in manufacturing-process optimization when flexible nonlinear approximation or explicit quantification of predictive uncertainty is required [32, 33]. These surrogate models are commonly coupled with evolutionary multi-objective optimization algorithms, for example, GA, PSO, and NSGA-II, to explore trade-offs between conflicting objectives and to obtain Pareto-optimal solutions [3, 11, 27, 31, 33, 34]. Such a strategy can reduce experimental cost and also improve process understanding, at least at the engineering level.

More recently, artificial neural networks, random forest models, and other data-driven approaches have been increasingly explored for machining response prediction because of their ability to capture complex nonlinear relationships [3, 31]. When sufficiently informative datasets are available, these approaches may achieve higher predictive accuracy than low-order polynomial models. However, their performance is strongly influenced by the quantity and representativeness of the training data, model architecture, or hyperparameter selection, and the adopted validation strategy. In contrast, RSM remains particularly suitable for structured, relatively small DOE datasets when the research objective extends beyond prediction to include factor significance, interaction interpretation, model transparency, and direct linkage to machining physics. Therefore, the present selection of RSM is based on the characteristics of the experimental design and the intended statistical and physical interpretation, rather than on an assumption that RSM universally outperforms black-box or probabilistic models.

However, despite these advances, the reporting of model adequacy, predictive generalization, and domain validity remains inconsistent in surrogate-assisted machining optimization studies. In many cases, surrogate models are primarily treated as numerical tools for response visualization or direct optimization, while issues such as residual behavior, multicollinearity, prediction error, model-domain restrictions, and independent confirmation receive comparatively limited attention. As a result, inaccuracies in the fitted response functions may propagate into the optimization stage and distort the location, shape, or interpretation of the resulting Pareto front. This concern is particularly relevant in multi-objective optimization because relatively small prediction errors in individual responses may alter the apparent balance among conflicting objectives.

Furthermore, some studies interpret the importance of machining parameters mainly through p-values or percentage contributions without sufficiently relating the statistically identified effects to the physical mechanisms governing surface generation, heat production, lubricant penetration, and interfacial friction. This approach risks interpreting statistical correlation as physical causation, thereby limiting the scientific depth and industrial relevance of the conclusions [4, 35-37]. A more straightforward integration of machining physics, statistically sound surrogate modeling, and decision-oriented optimization still lacks systematic exploration, especially for nanofluid MQL machining of hardened steels.

To address these gaps, the present study proposes a statistically validated multi-objective optimization framework for sustainable hard turning of heat-treated AISI 4140 steel using coconut oil-based MQL enhanced with CuO nanoparticles. The RSM models are evaluated through analysis of variance, residual diagnostics, multicollinearity assessment, prediction-error analysis, and experimental confirmation before being employed as objective functions in the optimization procedure. The statistically assessed models are subsequently integrated with NSGA-II to minimize

the risk that the resulting Pareto solutions are influenced by poorly fitted response relationships or unsupported extrapolation. The statistically significant effects are also interpreted using thermo-mechanical and tribological mechanisms to connect the empirical relationships with the physics of hard turning.

The objectives of this study are threefold: (i) to develop and statistically evaluate RSM models for surface roughness and cutting temperature within the investigated nanofluid-MQL hard-turning domain; (ii) to interpret the dominant main and interaction effects by combining statistical evidence with the physical mechanisms governing surface formation and thermal behavior; and (iii) to integrate the RSM predictions for surface roughness and cutting temperature with the analytically calculated material removal rate in an NSGA-II framework, thereby generating Pareto-optimal machining regimes and experimentally validating selected solutions. The study aims to enhance the methodological transparency of surrogate-assisted machining optimization and to provide practical decision support for balancing surface quality, thermal control, and productivity in sustainable hard turning.

2. Materials and Methodology

The workpiece material used in this investigation was AISI 4140 steel. Cylindrical specimens with a length of 115 mm and a diameter of 60 mm were prepared and then heat-treated to obtain a hardness of about 40 HRC (as depicted in Figure 1). The Taguchi L27 orthogonal array was employed to investigate the effects of cutting speed, feed rate, and depth of cut through 27 distinct machining conditions. The experiments were conducted in a randomized order, and a fresh cutting edge was used for each test to minimize systematic effects associated with progressive tool wear. The cutting length used to obtain the responses reported in the DOE dataset was approximately 50 mm. Therefore, repeated roughness readings taken from the same machined surface were used only to reduce local measurement variability and were not treated as independent experimental replications.

The nanofluid for MQL application was prepared by dispersing CuO nanoparticles into coconut oil. Since the MQL air pressure was maintained at 3 bar throughout the tests, the independent effect of pressure on tribofilm formation cannot be inferred from the present dataset. The average diameter of the CuO particles was about 20 nm, and their shape was examined by scanning electron microscopy (SEM), as shown in Figure 2. The nanoparticles were mixed with coconut oil at a concentration of 0.5 wt % [14, 20-23, 36, 38, 39]. The nanoparticle concentration was fixed at 0.5 wt% to isolate the effects of the three machining parameters within the L27 design. This concentration is not claimed to be globally optimal, and concentration-dependent optimization remains outside the scope of the present study.

A magnetic stirrer (MS-11C, Taiwan) was operated at 800 rpm for 48 h to promote the dispersion of CuO nanoparticles in coconut oil before the machining experiments. The same preparation procedure was consistently applied throughout the experimental campaign to minimize variations associated with nanofluid preparation. Because zeta potential, sedimentation behavior, and time-dependent viscosity were not quantitatively evaluated, the long-term colloidal stability of the prepared nanofluid was not established in the present study.

AISI 4140 is a medium-carbon alloy steel whose typical chemical composition is as follows: 0.38–0.43% C, 0.75–1.00% Mn, 0.80–1.10% Cr, 0.15–0.25% Mo, 0.15–0.40% Si, and P and S limited to 0.04% and 0.05%, respectively. This alloying system provides relatively high strength, good toughness, and wear resistance, as well as thermal stability. Therefore, AISI 4140 is widely used for gears, shafts, and other components subjected to heavy loading conditions.

The cutting parameters were selected based on previous research and recommendations from tool manufacturers. Cutting speed (v), feed rate (f), and depth of cut (a) were chosen as input variables. Table 1 summarises the levels of these factors considered. In the L27 array, three factors at three levels are arranged so that the effects of the main factors and their interactions can be estimated with a limited number of experiments.



Fig. 1. The AISI 4140 steel was used for all machining tests

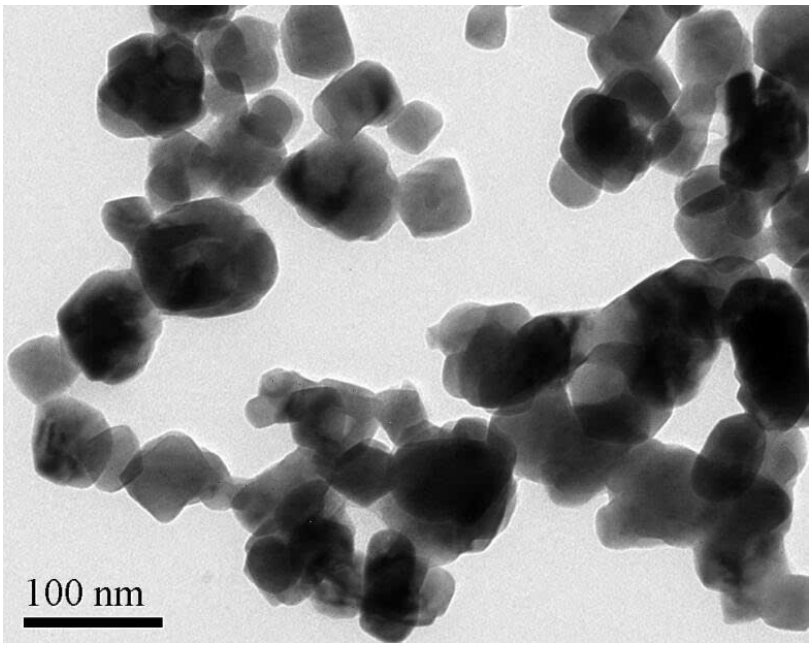


Fig. 2. SEM micrograph of CuO nanoparticles showing an average particle size of 20 nm, used for MQL lubrication

Table 1. The input parameters of the hard turning operation

Parameters	Variable	Units	Level 1	Level 2	Level 3
Cutting velocity (v)	x_1	m/min	100	125	150
Feed (f)	x_2	mm/rev	0.15	0.25	0.35
Depth of cut (a)	x_3	mm	0.2	0.3	0.4

All turning tests were carried out on a DMG CTX 310 ECO lathe. This machine allows a maximum turning diameter of 200 mm, a turning length of 393 mm, and a maximum spindle speed of 5000 rpm. A TNMG160404-CBN insert supplied by DASAN was used for semi-finishing to finishing operations on hardened materials. The insert has a neutral rake angle and a nose radius of 0.4 mm. The tool holder MTJNR 2020K16 was selected for this insert in order to ensure sufficient rigidity during cutting. The experimental set-up, including the MQL system and the cooling–lubrication arrangement, is illustrated in Figure 3.

Surface roughness and cutting temperature were chosen as the leading quality indicators in this work. Ra was measured using a Mitutoyo Surftest SJ-210 with a cut-off length of 0.8 mm. The stylus traversed perpendicular to the machining marks. Three measurements were taken at different circumferential positions, and their arithmetic mean was used for modeling.

The UNI-T UTi260 thermal camera was fixed approximately 1.5 m from the cutting zone and directed toward the region encompassing the tool tip and the immediate tool–workpiece contact area. An emissivity value of 0.20 was maintained for all tests. The camera position, viewing geometry, and measurement settings were kept unchanged throughout the experiments. The thermal-camera display was video-recorded, and the highest displayed temperature during the predefined cutting interval was extracted by frame-by-frame review. Accordingly, T_c represents the maximum apparent temperature recorded under consistent optical conditions rather than the true instantaneous interfacial temperature. Because no independent emissivity calibration against a contact-temperature reference was available, the measurements are interpreted primarily on a comparative basis.

MRR in turning was evaluated based on the kinematic–geometric relationship of chip removal. Given the cutting speed v (m/min), depth of cut a (mm), and feed rate f (mm/rev), MRR (cm^3/min) was obtained as:

$$MRR = v\ a\ f \tag{1}$$

For each trial, MRR was computed directly from the prescribed cutting parameters and was used as a measure of machining productivity in the subsequent analysis and optimization.

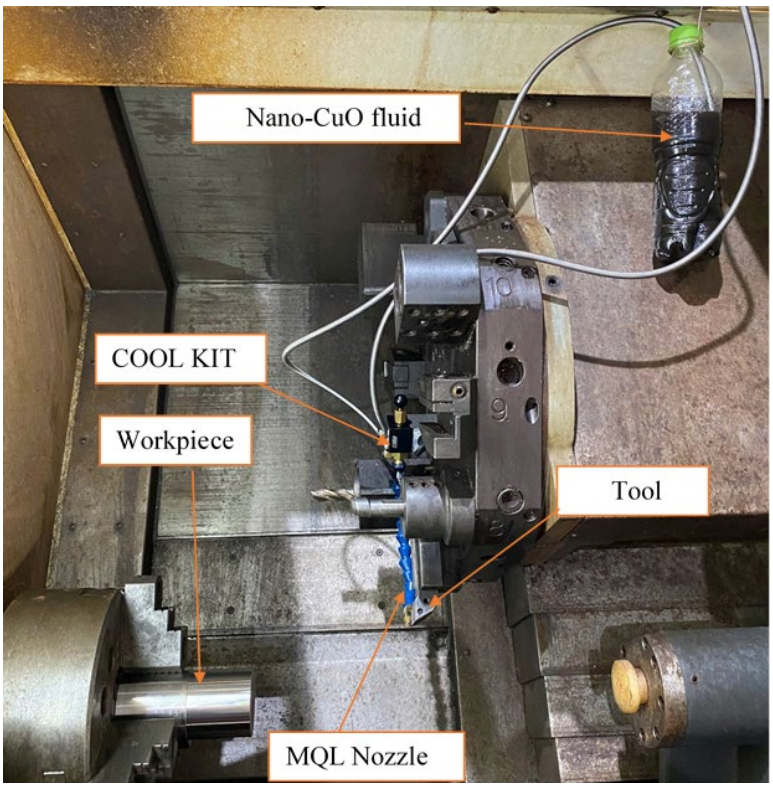


Fig. 3. Implementation and utilization of nanofluid MQL in the turning process

The optimization procedure consisted of two stages. First, second-order RSM models were developed only for the experimentally measured responses Ra and Tc. MRR was not modeled using RSM; instead, it was calculated analytically from the prescribed cutting speed, feed rate, and depth of cut using Eq. (1). Second, the statistically assessed RSM predictions for Ra and Tc and the analytical MRR relationship were integrated into the NSGA-II framework to minimize Ra and Tc while maximizing productivity. This distinction prevents the deterministic productivity relationship from being incorrectly interpreted as an experimentally fitted surrogate model. The complete workflow, from nanofluid preparation, machining experiments, response measurement, RSM modelling to multi-objective optimization, is presented in Figure 4.

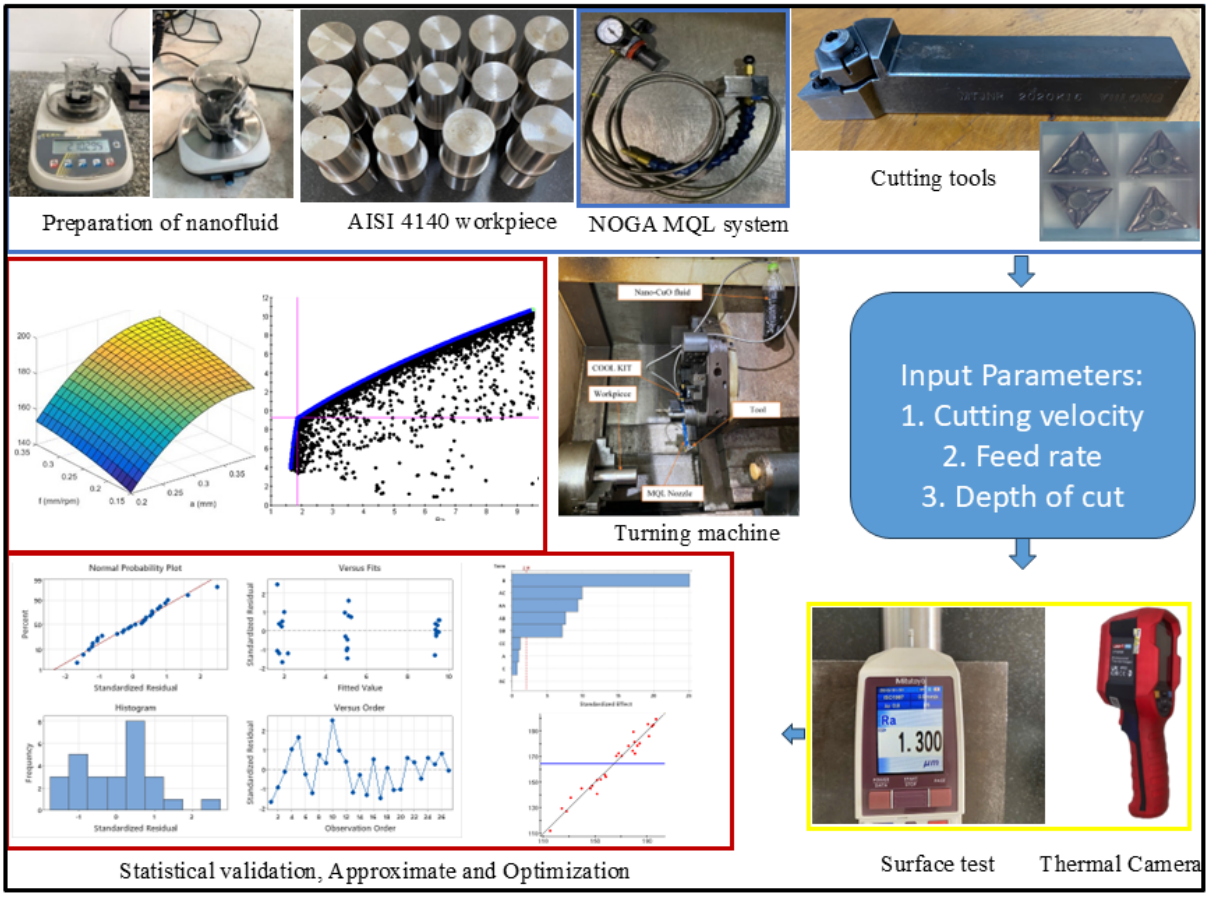


Fig. 4. Comprehensive research methodology framework

3. Results and Discussion

3.1 Experimental Results and Data Characteristics

Table 2 summarizes the combinations of cutting parameters and the corresponding measured responses from the 27 hard-turning experiments conducted on hardened AISI 4140 steels using a CuO nanofluid MQL based on coconut oil. The experimental results reveal substantial variations in machining performance: surface roughness ranges from approximately 1.55 µm to nearly 9.7 µm, cutting temperature varies between about 112 °C and 199 °C, and material removal rate (*MRR*) spans from 3 to 21 cm^3/min, depending primarily on feed rate and depth of cut.

The broad response ranges indicate a strong sensitivity of machining performance to process parameters, providing a sufficiently rich dataset for developing empirical surrogate models. Moreover, the experimental design ensures balanced coverage of the factor space, enabling reliable estimation of linear, quadratic, and interaction effects required for response surface modeling.

3.2 Development and Statistical Validation of Response Surface Models

Before physical interpretation and multi-objective optimization, the adequacy and predictive performance of the quadratic RSM models developed for Ra and Tc were systematically assessed. The models yielded R^2, adjusted R^2, and predicted R^2values exceeding 96% for both responses (Tables S1 and S2). In particular, the close agreement between adjusted and predicted R^2indicates that no pronounced deterioration in predictive performance was detected within the investigated design domain. Because the experimental design did not include independently replicated treatment combinations, pure error could not be estimated separately from residual error, and a conventional lack-of-fit test was therefore not claimed. Model assessment instead relied on ANOVA, PRESS-based prediction statistics, residual diagnostics, multicollinearity analysis, and confirmation experiments.

Table 2. The input variables and output variables of the turning of AISI 4140 steel

No.	v (m/min)	a (mm)	f (mm/rev)	Ra (μm)	Tc (^{0}C)	$MRR\ cm^3/min$
1	100	0.2	0.15	1.706	137.9	3.00
2	100	0.2	0.25	4.948	129.6	5.00
3	100	0.2	0.35	9.363	112.1	7.00
4	100	0.3	0.15	2.137	172.5	4.50
5	100	0.3	0.25	5.347	172.7	7.50
6	100	0.3	0.35	9.349	154.2	10.50
7	100	0.4	0.15	2.042	199.4	6.00
8	100	0.4	0.25	5.338	186.1	10.00
9	100	0.4	0.35	9.482	178.5	14.00
10	125	0.2	0.15	1.980	145.2	3.75
11	125	0.2	0.25	5.064	141.0	6.25
12	125	0.2	0.35	9.390	147.2	8.75
13	125	0.3	0.15	1.587	181.5	5.63
14	125	0.3	0.25	4.927	180.4	9.38
15	125	0.3	0.35	9.145	189.5	13.13
16	125	0.4	0.15	1.965	195.5	7.50
17	125	0.4	0.25	4.861	195.1	12.5
18	125	0.4	0.35	9.370	193.8	17.5
19	150	0.2	0.15	1.551	127.3	4.50
20	150	0.2	0.25	4.905	145.2	7.50
21	150	0.2	0.35	9.608	151.7	10.50
22	150	0.3	0.15	1.781	152.2	6.75
23	150	0.3	0.25	4.985	170.6	11.25
24	150	0.3	0.35	9.575	174.6	15.75
25	150	0.4	0.15	1.887	155.7	9.00
26	150	0.4	0.25	5.225	170.7	15.00
27	150	0.4	0.35	9.512	178.7	21.00

Based on the DOE results, full quadratic RSM equations were established to describe Ra and Tc as functions of cutting speed v, feed rate f, and depth of cut a, as given in Eqs. (2) and (3). Figure 5 compares the experimental and fitted values, whereas the model generalization capability was assessed separately using PRESS-based leave-one-out cross-validation, as summarized in Table S3. Predicted-versus-experimental plots (Figure 5) exhibit a close alignment along the unity line, without systematic deviation, which again confirms the robustness of the surrogate models.

$$\begin{aligned} Ra =& \mathrm{2.77\ -\ 0.0565\ v\ +\ 1.43\ a\ +\ 6.22\ f\ +\ 0.000192\ } \\ & \mathrm{v}^2\mathrm{\ +\ 2.95\ }\mathrm{a}^2\mathrm{\ +\ 56.83\ f}\mathrm{\ }^2\mathrm{-\ 0.0095\ v} \\ & * a\mathrm{+\ 0.0389\ v} * f\mathrm{\ -\ 5.45\ a} * f\mathrm{} \end{aligned} \quad (2)$$

$$\begin{aligned} Tc =& \mathrm{-360.8\ +\ 5.847\ v\ +\ 1349\ a\ -\ 456\ f\ -\ 0.02388\ } \\ & \mathrm{v}^2\mathrm{\ -\ 1143\ }\mathrm{a}^2 \\ & \mathrm{\ -\ 196\ }\mathrm{f}^2\mathrm{\ -\ 3.450\ v} \\ & * a\mathrm{+\ 4.493\ v} * f\mathrm{\ -\ 2\ a} * f\mathrm{} \end{aligned} \quad (3)$$

Predictive performance was further evaluated using PRESS-based leave-one-out cross-validation. For linear-in-parameter RSM models, the PRESS residuals are equivalent to prediction residuals obtained when each observation is excluded in turn from model estimation. For Ra, the PRESS value was 1.04492, corresponding to a predicted R^2 of 99.60%, an LOOCV RMSE of 0.197 μm, and an LOOCV MAE of 0.161 μm. For Tc, PRESS was 570.272, with a predicted R^2 of 96.06%, an LOOCV RMSE of 4.596 °C, and an LOOCV MAE of 3.627 °C. The agreement between adjusted and predicted

R^2, together with the cross-validated prediction errors, indicates that no substantial loss of predictive performance was detected within the experimental factor space. However, these internal cross-validation results should not be interpreted as a substitute for a large independently replicated validation dataset. Residual diagnostics were examined to assess the principal regression assumptions. As shown in Figure 6 for Ra and Figure 7 for Tc, the normal probability plots indicate that the residual distributions are approximately normal.

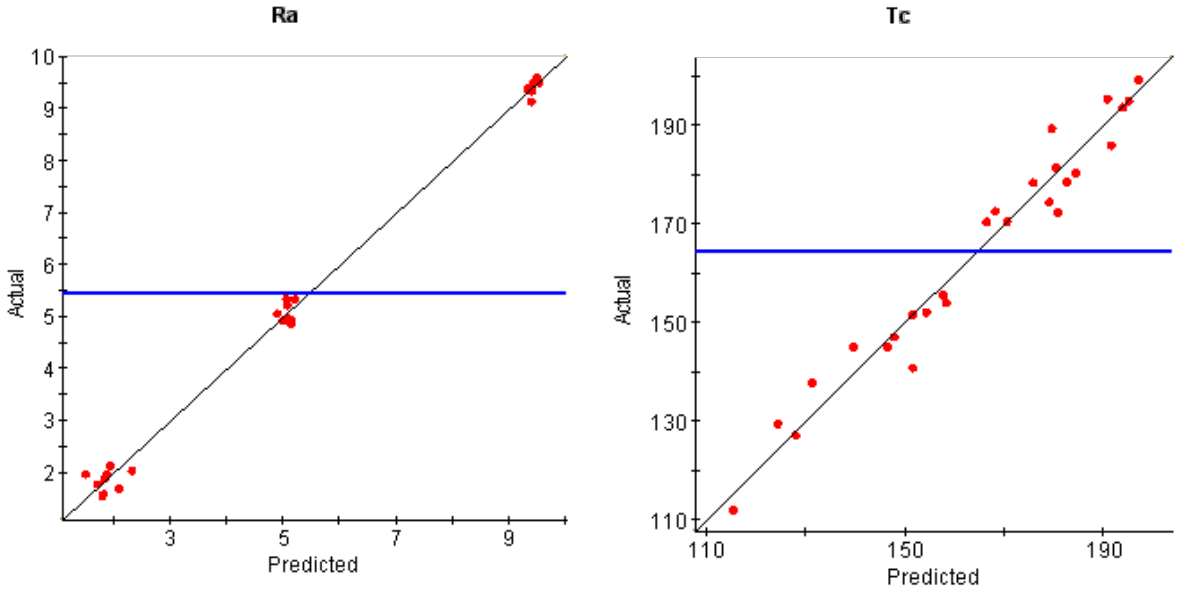


Fig. 5. Experimental versus fitted values for the RSM models: (a) surface roughness and (b) cutting temperature

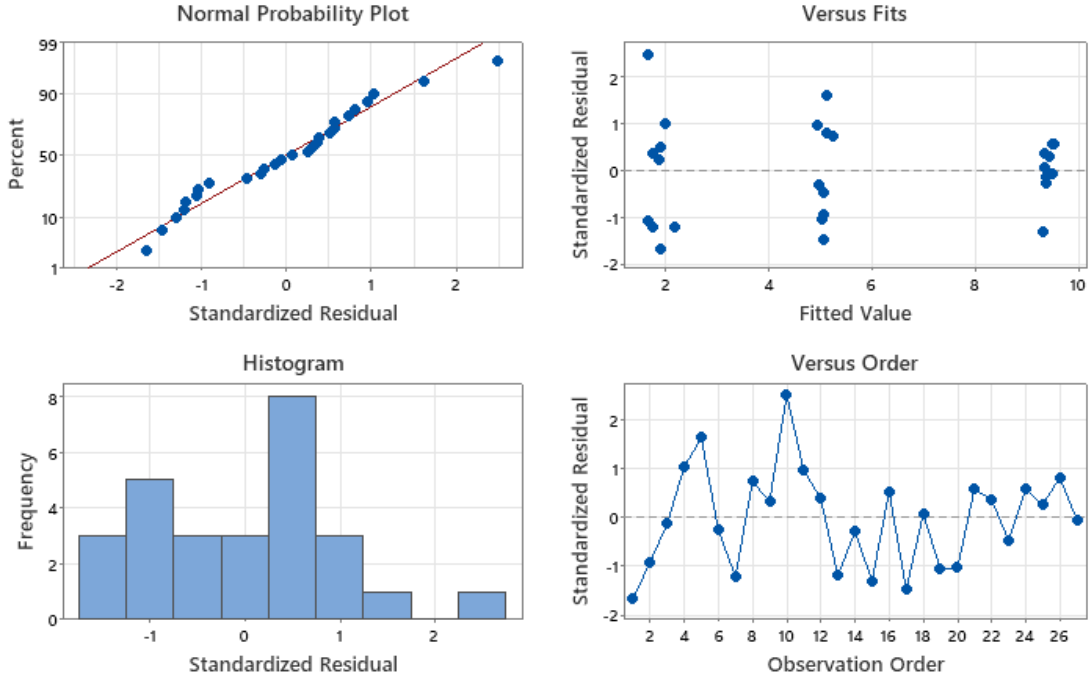


Fig. 6. Residual diagnostics used to assess approximate normality, variance stability, and run-order dependence for the Ra response surface model

The residuals-versus-fitted plots show no pronounced funnel-shaped or systematic pattern, while the residuals plotted against run order do not reveal an evident monotonic drift. The visual assessment of variance stability was supplemented by the Breusch–Pagan and White tests. The corresponding p-values were 0.201 and 0.525 for Ra and 0.645 and 0.764 for Tc, respectively. Thus, no statistically significant evidence of heteroscedasticity was detected at the 5% level within the

investigated domain. Nevertheless, the conventional RSM framework represents the conditional mean response and does not explicitly model input-dependent noise.

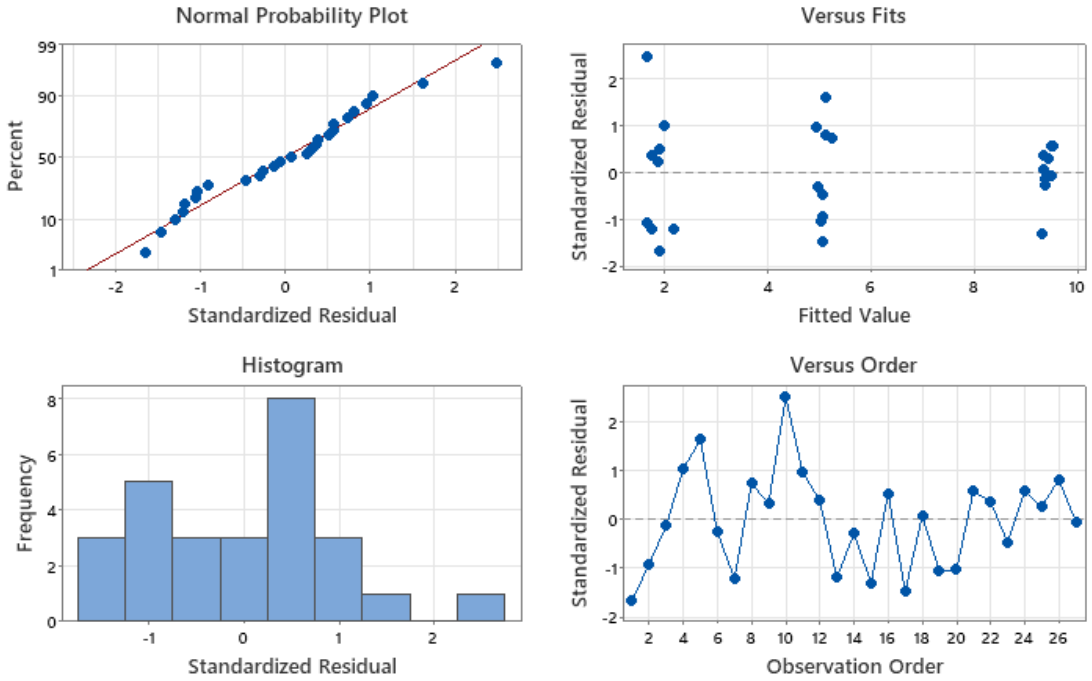


Fig. 6. Residual diagnostics used to assess approximate normality, variance stability, and run-order dependence for the Ra response surface model

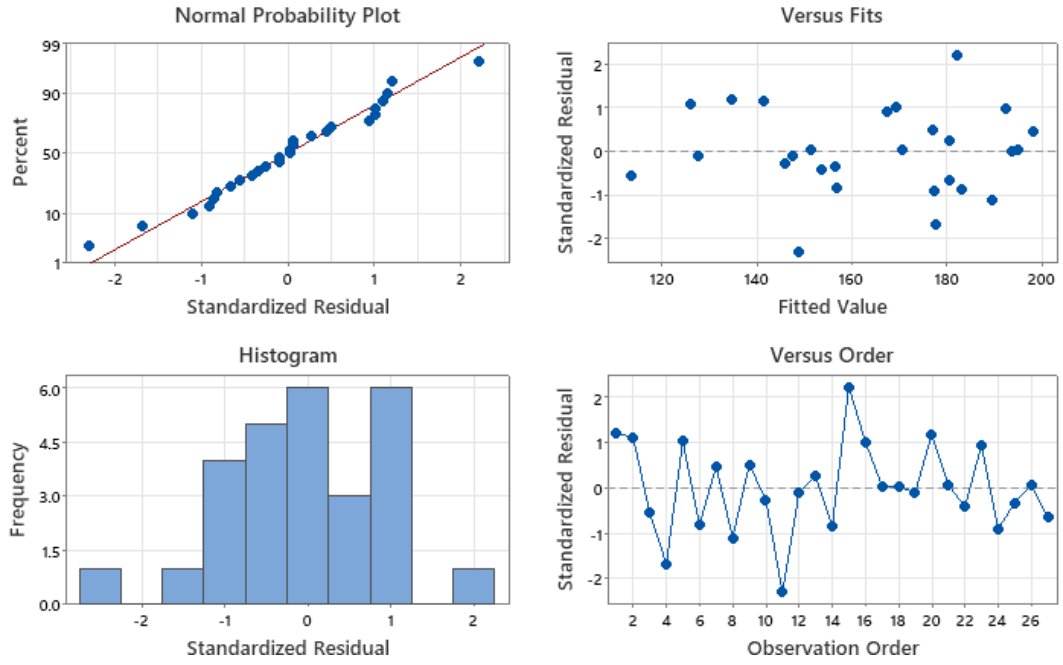


Fig. 7. Residual diagnostics used to assess approximate normality, variance stability, and run-order dependence for the Tc response surface model

Additional regression diagnostics also support the model's robustness. All variance inflation factor (VIF) values are equal to unity, indicating no problematic multicollinearity in the coded-variable formulation (see Tables S4 and S5). Collectively, these results indicate that the developed surrogate models are statistically sound and suitable for subsequent physical interpretation and multi-objective optimization.

3.3 Influence of Machining Parameters on Surface Roughness and Cutting Temperature

The global effects of input parameters on Ra and Tc are illustrated in Figure 8. For surface roughness, feed rate is clearly the most influential factor, as reflected by the steepest gradient. When feed increases from 0.15 to 0.35 mm/rev, Ra rises rapidly in a near-monotonic manner. Cutting speed shows a secondary influence, whereas depth of cut has the weakest effect within the investigated range. This behaviour suggests that, during nanofluid MQL hard turning, surface roughness is mainly governed by feed-related mechanisms (geometric and tribological).

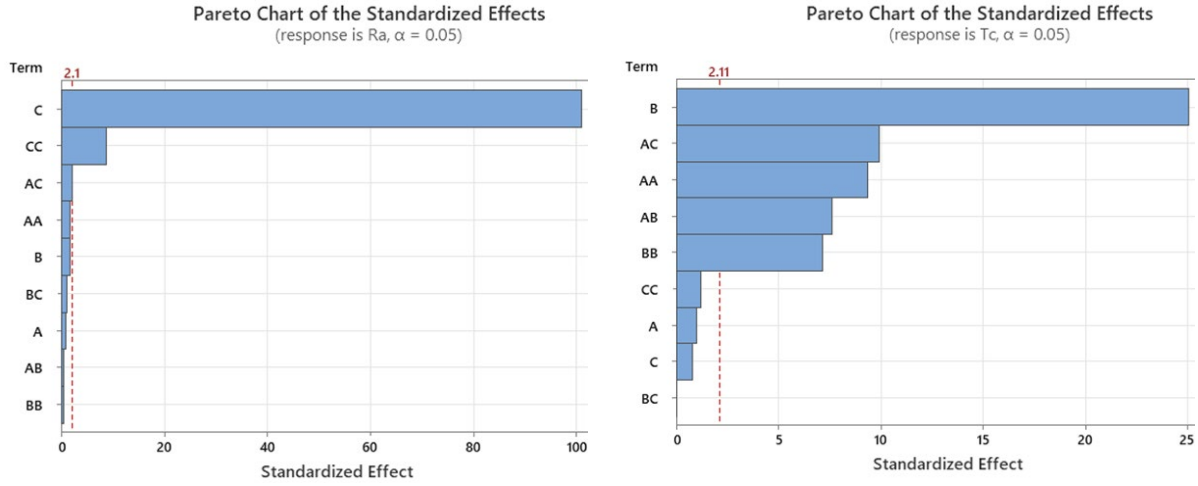


Fig. 8. Pareto charts of standardized effects for (a) Ra and (b) Tc

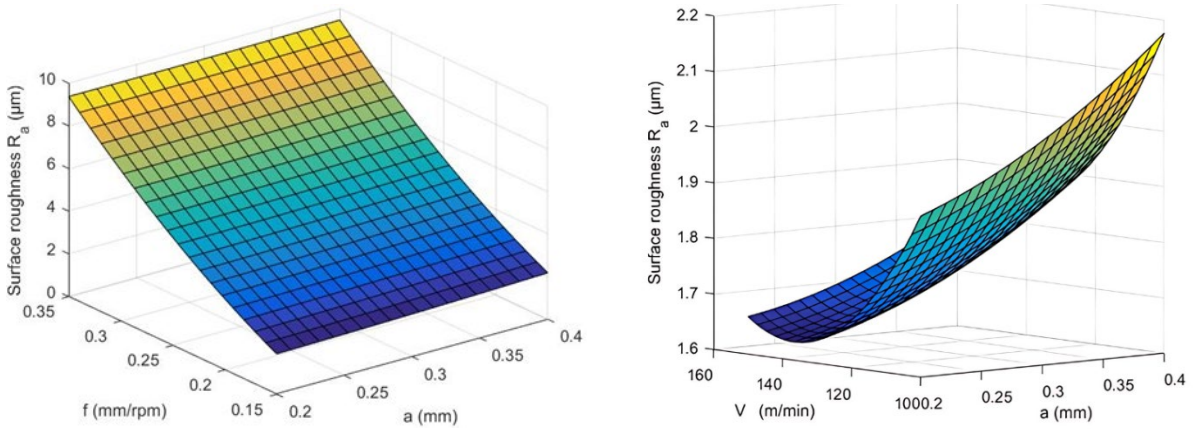


Fig. 9. Response surface plots for surface roughness

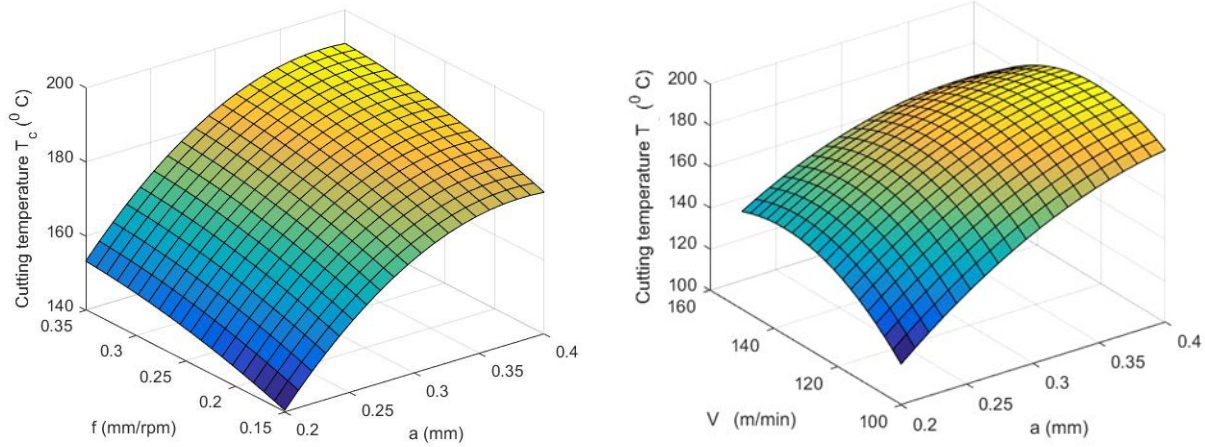


Fig. 10. Response surface plots for cutting temperature

In contrast, cutting temperature presents a different sensitivity pattern. Depth of cut exerts the most potent effect on Tc, followed by cutting speed, while feed rate has a comparatively weaker influence. Increasing the depth of cut from 0.20 to 0.40 mm leads to a pronounced increase in cutting temperature, attributed to an enlarged tool–workpiece contact area and more substantial plastic deformation in the primary shear zone. Therefore, thermal load is more closely related to engagement conditions than to purely kinematic surface generation.

To further illustrate interaction effects, three-dimensional response surfaces for Ra and Tc were constructed, as shown in Figures 9 and 10, respectively. Figure 9a indicates that Ra increases sharply with feed rate, while it remains relatively insensitive to depth of cut. Figure 9b reveals a distinct nonlinear relationship between cutting speed and Ra: Ra decreases as cutting speed increases from 100 to around 130 m/min, reaching a minimum of approximately 1.65–1.70 μm, and then increases again at higher speeds. This U-shaped trend may reflect a transition from unstable cutting at low speeds to a more favorable shearing regime at intermediate speeds and then to thermal accumulation and dynamic disturbances when cutting speed becomes too high.

For Tc (Fig. 10), the dominant role of depth of cut is clearly observed. Increasing feed rate causes only a moderate rise in Tc (about 20 °C across the studied range), whereas increasing depth of cut results in an increase exceeding 50 °C. The nonlinear dependence of Tc on cutting speed is likely due to competing effects: higher speed increases heat generation, but under nanofluid MQL, it may also enhance heat removal and reduce friction at the interface. Overall, it can be concluded that Ra and Tc are controlled by fundamentally different mechanisms: Ra is dominated by feed-related geometric/tribological effects, while Tc is mainly governed by volumetric deformation and thermal load.

3.4 ANOVA-Based Interpretation and Physical Mechanisms

ANOVA results provide further evidence for the governing mechanisms. For surface roughness, ANOVA (Table S6) indicates that feed-related terms account for 99% of the total variance ($p < 0.001$). The statistically significant quadratic term for feed rate (f^2, $p < 0.001$) indicates a pronounced nonlinear effect, with Ra increasing disproportionately as feed rate increases. In addition, the significant interaction term ($v \times f$, $p < 0.05$) indicates that the influence of feed on surface integrity is modulated by cutting speed, which is reasonable, as chip formation dynamics and tool–workpiece interaction change with speed.

From a physical viewpoint, increasing feed rate directly increases uncut chip thickness, which raises kinematic surface roughness and intensifies mechanical interaction at the tool–workpiece interface. At higher feed rates, the lubricating film formed by the coconut oil–CuO nanofluid becomes less effective due to reduced residence time and increased contact pressure, thereby limiting the nanoparticles' ability to form stable tribofilms or act as rolling and mending agents. Consequently, surface finish deteriorates quickly even in the presence of nanofluid MQL [13, 15, 17, 18, 35, 36, 39-42].

For cutting temperature, ANOVA (Table S7) shows that depth of cut is the dominant factor, contributing approximately 66.6% of the total variance ($p < 0.001$). Significant quadratic effects of cutting speed and depth of cut confirm the nonlinear thermal response in the cutting zone. Moreover, significant interaction terms ($v \times f$ and $v \times a$) suggest coupled kinematic–thermal effects, arising from the combined influence of cutting speed and chip load. These findings also explain why nanofluid MQL, while effective at reducing friction, still cannot fully offset the increased heat generation under high engagement conditions. The proposed thermo-mechanical and tribological mechanisms provide physics-based interpretations of the statistically significant effects; however, direct tribofilm chemistry, contact-zone microscopy, and tool-surface characterization were not performed. Accordingly, these mechanisms should be interpreted as literature-supported explanations rather than direct experimental verification of tribofilm formation.

An order-of-magnitude Peclet number was estimated as $Pe = vc\ h/\alpha$, where vc is cutting speed, h is represented by the uncut chip thickness, and α is the thermal diffusivity. Based on the investigated ranges, Pe is approximately 23–81, indicating a relatively high-Peclet regime in which heat

transport by the moving chip/material is important relative to thermal diffusion [43]. This estimate is used only for physical interpretation and is not a direct thermal measurement.

3.5 Multi-Objective Optimization and Pareto-Based Decision Analysis

After constructing and statistically evaluating the RSM models, multi-objective optimization was performed to minimize Ra and Tc while simultaneously maximizing MRR. The resulting Pareto fronts are less likely to be affected by gross model inadequacy because the surrogate models were assessed before optimization; however, they remain nominal deterministic trade-offs within the investigated design space.

Using NSGA-II (with parameters set to a crossover distribution index of 10.0, crossover probability of 0.9, mutation distribution index of 20.0, population size of 40, and 120 generations), Pareto-optimal solutions were generated within the experimental bounds. Fig. 11 shows the Pareto front for minimizing Ra and maximizing MRR, with two distinct zones. In the first zone (Ra ≈ 1.5–1.9 μm), a small sacrifice in surface quality results in a substantial increase in productivity, which is highly attractive for many applications. In the second zone (Ra > 1.9 μm), further increases in Ra yield only marginal improvements in MRR, indicating diminishing returns. Because repeated Isight runs with different random seeds and a formal parameter-sensitivity analysis were not retained, no statistical claim is made regarding run-to-run convergence repeatability or insensitivity to the selected NSGA-II configuration; the reported fronts should therefore be interpreted as nominal solutions obtained using the disclosed fixed settings.

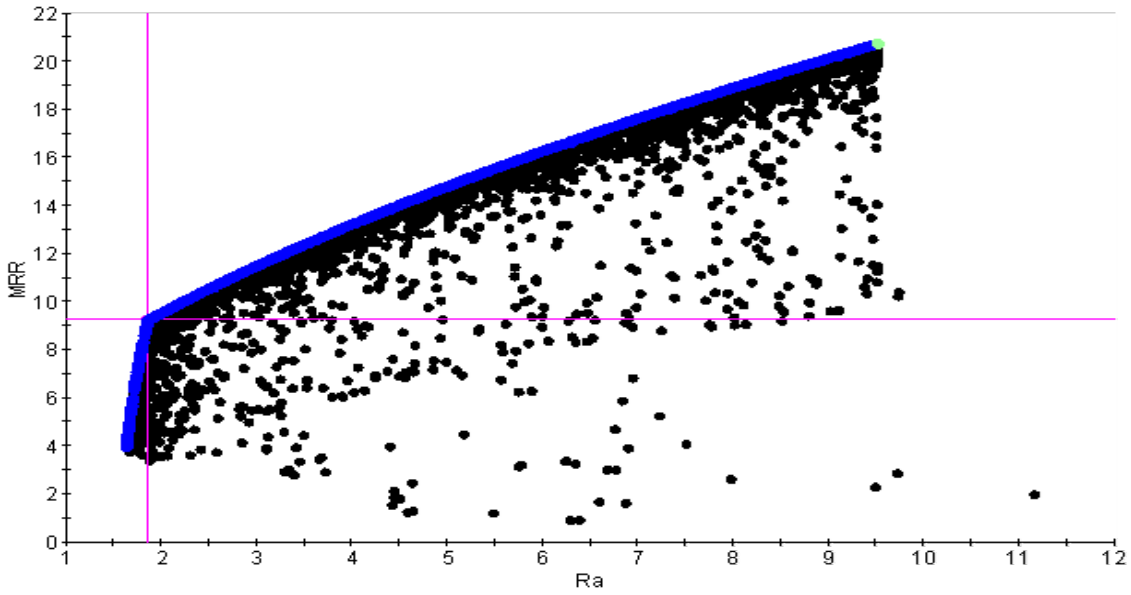


Fig. 11. Pareto front generated by the combination of RSM and NSGA-II for maximum MRR and minimum Ra

For cases where both surface quality and productivity are required, a compromise solution (Ra = 1.969 μm and MRR = 9.243 cm^3/min) was selected. At this point, the CuO-coconut oil nanofluid MQL provides sufficient lubrication and cooling to maintain acceptable surface integrity while still achieving a relatively high productivity. To address semi-finishing requirements, an additional constrained optimization was performed, limiting Ra to 1.6–3.2 μm while simultaneously minimizing Tc and maximizing MRR. The resulting Pareto front is presented in Figure 12. Two representative solutions were selected from this constrained front. The surface-quality-prioritized regime provides Ra = 1.668 μm, Tc = 127.579 °C, and MRR = 4.5 cm^3/min, offering a lower measured thermal load, although tool-wear behavior was not directly evaluated, but at lower productivity (point A). On the other hand, the productivity-prioritized regime achieves Ra = 3.20 μm, Tc = 163.4 °C, and MRR = 11.727 cm^3/min (point B), delivering nearly 2.8 times higher productivity, but with increased surface roughness and cutting temperature.

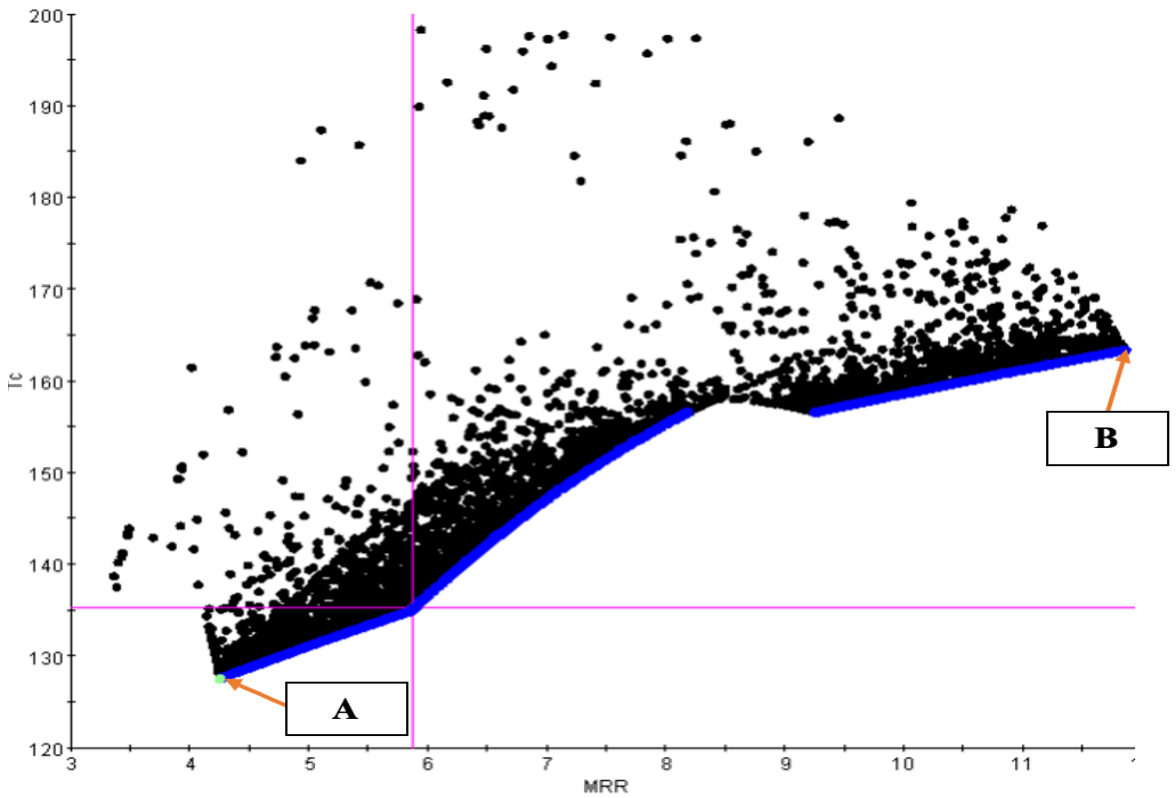


Fig. 12. Optimal balance curve between thermal control and productivity under semi-finishing Ra constraints

From a practical viewpoint, the selection between these regimes depends on production objectives and constraints. When tool cost and downtime are critical, the surface-quality-prioritized regime is preferable due to lower thermal load. Meanwhile, for high-volume production, a productivity-oriented regime can be selected, provided that the resulting Ra and Tc remain acceptable for the intended component function. In this way, the proposed framework does not give a single "best" point, but rather a set of physically interpretable candidate solutions to support decision-making in sustainable hard turning.

Confirmation experiments were conducted at three representative decision regimes selected from different regions of the Pareto solutions: a surface-quality-prioritized regime (V1), a productivity-prioritized regime (V2), and a compromise regime (V3). The decision variables generated by the optimizer were rounded to practically implementable machine settings before the confirmation tests. To maintain consistency, the RSM predictions for Ra and Tc were recalculated at these implemented settings rather than retained from the original unrounded optimizer outputs. As presented in Table 3, the absolute relative errors ranged from 5.25% to 7.98% for Ra and from 3.21% to 7.93% for Tc. These results provide local confirmation of the predictive consistency of the RSM models at the selected operating points within the investigated factor domain. Because each selected condition was confirmed by a single machining run, the results should not be interpreted as a replicated estimate of process variability.

MRR was not modeled using RSM and was not independently validated as an experimental response. Instead, it was calculated analytically from the implemented cutting speed, feed rate, and depth of cut using Eq. (1). Therefore, no prediction error was assigned to MRR. The confirmation results demonstrate that the selected Pareto solutions are practically implementable and that the measured Ra and Tc values remain reasonably close to the corresponding model predictions. Nevertheless, these local confirmation tests do not eliminate the uncertainty associated with the surrogate models or the stochastic nature of NSGA-II; rather, they support the feasibility and predictive consistency of the selected decision regimes within the experimental bounds.

Table 3. Confirmation results at three representative Pareto decision regimes

Point	Optimization regime	v	f	a	Response	Model prediction/ analytical value	Experi-mental	Absolute Error (%)
V1	Surface-quality-prioritized	150	0.15	0.2	*Ra* (μm)	1.668	1.58	5.25
					Tc (^{0}C)	127.58	118.7	6.96
					MRR (cm^3/min)	4.5	-	-
V2	Productivity-prioritized	150	0.195	0.4	*Ra* (μm)	3.185	3.08	3.31
					Tc (^{0}C)	163.36	158.8	2.79
					MRR (cm^3/min)	11.70	-	-
V3	Compromise Pareto point	150	0.15	0.4	*Ra* (μm)	1.859	1.76	5.31
					Tc (^{0}C)	156.62	144.2	-7.9
					MRR (cm^3/min)	9.0	-	-

3.6 Scope Limitations and Extension to Advanced Materials

The present framework was developed for homogeneous heat-treated AISI 4140 steels, for which the mechanical and thermal properties were assumed to remain approximately uniform throughout the machined region. The same experimental–computational strategy could be extended to functionally graded materials (FGMs) and other heterogeneous material systems [44, 45]. In such materials, spatial variations in hardness, elastic–plastic properties, thermal conductivity, and reinforcement fraction may produce position-dependent cutting forces, surface integrity, temperature, and tool-wear behavior. Therefore, the local material state, graded-zone position, or relevant property descriptors would need to be introduced as additional model inputs, while the experimental design should include adequate sampling across the graded region. The resulting surrogate models could then be integrated with multi-objective optimization to identify machining conditions that account simultaneously for process performance and material-property gradients. However, this extension requires dedicated experiments and cannot be inferred directly from the present AISI 4140 dataset.

4. Conclusions

This study systematically investigates hard turning of heat-treated AISI 4140 steels using a coconut oil–based CuO nanofluid MQL strategy, aiming to improve surface integrity, control thermal load, and enhance productivity simultaneously. A structured experimental–computational framework was established by combining Taguchi L27 DOE, RSM, rigorous statistical validation, and multi-objective optimization using NSGA-II.

Comprehensive statistical diagnostics confirm that the developed quadratic surrogate models for *Ra* and *Tc* are robust and predictive. High coefficients of determination (R^2, adjusted R^2, and predicted $R^2 > 96\%$), together with residual diagnostics, the absence of multicollinearity, and stable regression behaviour, indicate that the subsequent physical interpretation and optimization are grounded on statistically sound models rather than numerical artefacts.

ANOVA-based analysis further reveals that *Ra* and *Tc* are governed by fundamentally different mechanisms. Surface roughness is overwhelmingly dominated by feed-related effects, especially the quadratic term of feed rate, implying a strong nonlinear deterioration of surface integrity at higher feed levels even in the presence of nanofluid-assisted MQL. In contrast, cutting temperature is mainly controlled by depth of cut, showing the strongest linear, quadratic, and interaction contributions due to its direct influence on shear zone size, tool–chip contact area, and volumetric heat generation. These statistically supported findings are also consistent with physical explanations, including kinematic roughness formation, stability of nanoparticle-induced tribofilms, and dissipation of thermomechanical energy in the cutting zone.

By integrating the validated RSM models with NSGA-II, Pareto fronts were generated to explicitly quantify trade-offs among surface quality, thermal behaviour, and material removal rate. A

compromise point ($Ra \approx 1.969$ μm and $MRR \approx 9.24$ cm^3/min) was identified, where a marginal sacrifice in surface finish can provide a substantial gain in productivity. Moreover, two practically relevant regimes were extracted: (i) a surface-quality-prioritized regime with low *Ra* and reduced cutting temperature, which reduces the measured thermal load and may support dimensional stability, although tool wear was not measured; and (ii) a productivity-prioritized regime delivering nearly threefold higher *MRR* at the cost of increased thermal load and higher surface roughness. In this way, the proposed framework provides machining practitioners not only with a single deterministic setting but also with a set of physically interpretable and application-oriented decision options.

Overall, the results demonstrate the feasibility of balancing surface roughness, cutting temperature, and analytical productivity under the investigated MQL condition using coconut oil CuO nanofluid. Because no base-MQL control was included, the present results should not be interpreted as a direct experimental demonstration of the superiority of nanofluid MQL over the unmodified base oil. More importantly, the statistically validated RSM–NSGA-II framework offers a robust methodology for linking experimental evidence, physical interpretation, and multi-objective decision-making, and is readily extensible to other difficult-to-machine materials, cutting tools, and sustainable lubrication strategies. Future work should incorporate tool-wear evolution, subsurface integrity, nanoparticle concentration, direct comparison with base MQL, and uncertainty-aware optimization. The framework may also be extended to functionally graded and other heterogeneous materials by introducing the local material state or graded-zone position as additional model variables and by designing experiments that adequately represent spatial variations in mechanical and thermal properties.

Acknowledgment

Nha Trang University supported this work.

References

[1] Makhesana MA, Patel KM, Pimenov DY, Khanna N, Sarikaya M, Krolczyk GM. Machinability improvement and sustainability assessment during machining of AISI 4140 using vegetable oil-based MQL. J Braz Soc Mech Sci Eng. 2021;43(12):535. https://doi.org/10.1007/s40430-021-03250-7

[2] Ahmed W, Bisharat H, Al-Sultan S, Al-Wahaibi A, Al-Habsi S, Al-Maharbi M. Analysis and Optimization of Machining Hardened Steel AISI 4140 with Self-Propelled Rotary Tools. Materials (Basel). 2021;14(20):6106. https://doi.org/10.3390/ma14206106

[3] Meddour I, Yallese MA, Khattabi R, Elbah M, Mabrouki T. Prediction of surface roughness and cutting forces using RSM, ANN, and NSGA-II in finish turning of AISI 4140 hardened steel with mixed ceramic tool. Int J Adv Manuf Technol. 2018;97(5-8):1931-1949. https://doi.org/10.1007/s00170-018-2026-6

[4] Padhan S, Das A, Das SR, Alotaibi A, Alotaibi M, Mia M. Investigation on Surface Integrity in Hard Turning of AISI 4140 Steel with SPPP-AlTiSiN Coated Carbide Insert under Nano-MQL. Lubricants. 2023;11(2):49. https://doi.org/10.3390/lubricants11020049

[5] Mia M. Mathematical modeling and optimization of MQL assisted end milling characteristics based on RSM and Taguchi method. Measurement. 2018;121:249-260. https://doi.org/10.1016/j.measurement.2018.02.017

[6] Ali SH, Yip WS, To S. Recent developments in MQL machining of aeronautical materials: A comparative review. Chin J Aeronaut. 2025;38(1):102918. https://doi.org/10.1016/j.cja.2024.102918

[7] Ishfaq K, Ahmad S, Asad M, Pruncu CI, Khan AM, Maqsood MA. Progressing towards Sustainable Machining of Steels: A Detailed Review. Materials (Basel). 2021;14(18):5162. https://doi.org/10.3390/ma14185162

[8] Bhowmik A, Dey S, Ray A. A comprehensive review on the viability of minimum quantity lubrication technology for machining difficult-to-cut alloys. AIP Adv. 2025;15(3):030702. https://doi.org/10.1063/5.0245112

[9] Dastgerdi HM, Mousavi SA, Sharifi H. Comparative evaluation of dry, wet, and minimum quantity lubrication (MQL) cooling strategies in the machining of GTD-450 martensitic stainless steel. Sci Rep. 2026;16(1):1376. https://doi.org/10.1038/s41598-026-84123-4

[10] Junior ASA, da Silva RB, Machado AR, Hassui A. Tribological and dynamic behaviour in sustainable milling of SAE 1045 steel with plant-based lubrication. J Braz Soc Mech Sci Eng. 2026;48(1):54. https://doi.org/10.1007/s40430-025-05312-8

[11] Vu NC, Dang XP, Huang SC. Multi-objective optimization of hard milling process of AISI H13 in terms of productivity, quality, and cutting energy under nanofluid minimum quantity lubrication condition. Meas Control. 2021;54(5-6):820-834. https://doi.org/10.1177/00202940211013725
[12] Vu NC, Nguyen HT, Truong TT, Nguyen HT. Experimental and Metamodel Based Optimization of Cutting Parameters for Milling Inconel-800 Superalloy Under Nanofluid MQL Condition. Math Model Eng Probl. 2023;10(1):189-194. https://doi.org/10.18280/mmep.100122
[13] Zadafiya K, Patel K, Makhesana M. Recent advancements in nano-lubrication strategies for machining processes considering their health and environmental impacts. J Manuf Process. 2021;68:481-511. https://doi.org/10.1016/j.jmapro.2021.05.059
[14] Nguyen HT, Vu NC. Enhancing the Hard Turning Efficiency of 40Cr Alloy Steel with Coconut Oil-Based Nano-CuO Minimum Quantity Lubrication. Math Model Eng Probl. 2024;11(12):3280-3290. https://doi.org/10.18280/mmep.111208
[15] Khatai S, Sahoo AK, Panda A, Rout AK, Kumar A. Investigation on machinability and sustainability aspects during hard turning under GO nanofluid MQL environment for precision and cleaner manufacturing. Precision Eng. 2025;95:379-408. https://doi.org/10.1016/j.precisioneng.2025.04.012
[16] Pal A, Chatha SS, Sidhu HS. Tribological characteristics and drilling performance of nano-MoS2-enhanced vegetable oil-based cutting fluid using eco-friendly MQL technique in drilling of AISI 321 stainless steel. J Braz Soc Mech Sci Eng. 2021;43(4):189. https://doi.org/10.1007/s40430-021-02913-9
[17] Abellán-Nebot JV, Romero A, Vila C, Siller HR. Application of Hybrid Nanofluids in MQL Assisted Machining Operations: Exploring Synergies and Establishing Guidelines. Int J Precis Eng Manuf Green Technol. 2025;12(2):657-689. https://doi.org/10.1007/s40684-024-00621-x
[18] Javid H, Malik A, Ahmad S, Khan AM, Hussain S. Parametric analysis of turning HSLA steel under minimum quantity lubrication (MQL) and nanofluids-based minimum quantity lubrication (NF-MQL): a concept of one-step sustainable machining. Int J Adv Manuf Technol. 2021;117(5-6):1915-1934. https://doi.org/10.1007/s00170-021-07821-2
[19] Tiwari A, Singh DK, Mishra S. A review on minimum quantity lubrication in machining of different alloys and superalloys using nanofluids. J Braz Soc Mech Sci Eng. 2024;46(3):112. https://doi.org/10.1007/s40430-024-04689-0
[20] Jafarian Zenjanab M, Sarafraz M, Akbari M. Influence of Cutting Fluid-Based CuO-Nanofluid with Boric Acid-Nanoparticles Additives on Machining Performances of AISI 4340 Tool Steel in High-Speed Turning Operation. Iran J Sci Technol Trans Mech Eng. 2022;46(2):335-345. https://doi.org/10.1007/s40997-021-00438-7
[21] Virdi RL, Chatha SS, Singh H. Performance evaluation of nanofluid-based minimum quantity lubrication grinding of Ni-Cr alloy under the influence of CuO nanoparticles. Adv Manuf. 2021;9(4):580-591. https://doi.org/10.1007/s40436-021-00358-0
[22] Das A, Patel SK, Biswal BB. Processing of hardened steel by MQL technique using nano cutting fluids. Mater Manuf Process. 2021;36(3):316-328. https://doi.org/10.1080/10426914.2020.1843673
[23] Jhodkar D, Gupta K. Effect of CuO nanoparticles-based vegetable oil on the machining performance of WC tool insert while turning EN 8 steel. In: Proceedings of the International Conference on Industrial Engineering and Operations Management. Detroit: IEOM Society; 2020. p. 1240-1248.
[24] Hsiao TC, Vu NC, Huang SC, Dang XP. Modeling and optimization of machining parameters in milling of INCONEL-800 super alloy considering energy, productivity, and quality using nanoparticle suspended lubrication. Meas Control. 2021;54(5-6):880-894. https://doi.org/10.1177/00202940211013730
[25] Nguyen MQ, Vu NC, Dang XP. Experimental Model and Optimization of Cutting Parameters in Hard Milling SKD61 Steel Under Nanofluid MQL Environment. In: Long BT, Kim YH, Ishizaki T, editors. Advances in Engineering Research and Application. Cham: Springer; 2021. p. 325-334. https://doi.org/10.1007/978-3-030-64719-3_37
[26] Nguyen HT, Vu NC, Dang XP. Multi-objective Optimization of Cutting Parameters in CNC Turning for Surface Roughness and Productivity. In: Long BT, Kim YH, Ishizaki T, editors. Advances in Engineering Research and Application. Cham: Springer; 2022. p. 412-421. https://doi.org/10.1007/978-3-030-92574-1_45
[27] Vu NC, Truong TT, Nguyen HT. Experimental Investigation of Cutting Parameters in Machining of Inconel-800 Super-Alloy Under Nanofluid MQL Using Integrated RSM and NSGA-II. In: Long BT, Kim YH, Ishizaki T, editors. Advances in Engineering Research and Application. Cham: Springer; 2022. p. 422-431. https://doi.org/10.1007/978-3-030-92574-1_46
[28] Nguyen Huu T, Vu Ngoc C. Advancing turning performance of C45 steel for marine applications: A comprehensive study on optimizing cutting conditions. J Fish Sci Technol. 2024;2024(1):63-69. https://doi.org/10.54644/jte.2024.1521
[29] Kumar Parida A, Maity K. Modeling of machining parameters affecting flank wear and surface roughness in hot turning of Monel-400 using response surface methodology (RSM). Measurement. 2019;137:375-381. https://doi.org/10.1016/j.measurement.2019.01.070

[30] Mammeri S, Benhamena A, Yallese MA, Belhadi S. Filament manufacturing via external grooving of an HDPE pipe wall: RSM optimization and mechanical tests validation. Res Eng Struct Mater. 2025;11(1):73-96. https://doi.org/10.17515/resm2024.180ma0326
[31] Nguyen TT. Prediction and optimization of machining energy, surface roughness, and production rate in SKD61 milling. Measurement. 2019;136:525-544. https://doi.org/10.1016/j.measurement.2018.12.098
[32] Baum M, Anders D, Reinicke T. Optimizing injection molding simulations: comparative performance of Kriging and RSM surrogate models for process efficiency. Discover Mech Eng. 2025;4(1):31. https://doi.org/10.1007/s44245-025-00092-2
[33] Dang XP. Constrained multi-objective optimization of EDM process parameters using Kriging model and particle swarm algorithm. Mater Manuf Process. 2018;33(4):397-404. https://doi.org/10.1080/10426914.2017.1328111
[34] Prakash C, Kansal HK, Pabla BS, Puri S. Multi-objective parametric appraisal of pulsed current gas tungsten arc welding process by using hybrid optimization algorithms. Int J Adv Manuf Technol. 2019;101(1-4):1107-1123. https://doi.org/10.1007/s00170-018-2977-z
[35] Çakır Şencan A, Kılıçkap E, Yaşar N. Evaluation of machining characteristics of SiO2-doped vegetable-based nanofluids with Taguchi approach in turning of AISI 304 steel. Tribol Int. 2024;191:109122. https://doi.org/10.1016/j.triboint.2023.109122
[36] Usluer E, Kırbaş B, Akyüz B, Morkoç İ, Günay M. Investigation on the effect of hybrid nanofluid in MQL condition in orthogonal turning and a sustainability assessment. Sustain Mater Technol. 2023;36:e00618. https://doi.org/10.1016/j.susmat.2023.e00618
[37] Gupta MK, Mia M, Pruncu CI, Khan AM, Rahman MA, Jamil M, et al. Parametric optimization and process capability analysis for machining of nickel-based superalloy. Int J Adv Manuf Technol. 2019;102(9-12):3995-4009. https://doi.org/10.1007/s00170-019-03453-0
[38] Virdi RL, Chatha SS, Singh H. Processing Characteristics of Different Vegetable Oil-based Nanofluid MQL for Grinding of Ni-Cr Alloy. Adv Mater Process Technol. 2022;8(1):210-223. https://doi.org/10.1080/2374068X.2020.1809733
[39] ST PK, V N, Shanmugam S, S R. Investigate the effect of Al2O3 and CuO nano cutting fluids under MQL technique in turning of DSS-2205. Adv Mater Process Technol. 2022;8(3):3297-3330. https://doi.org/10.1080/2374068X.2021.1945228
[40] Somayajula SP, Sahoo AK, Panda A, Rout AK. Experimental investigation on performance of cryogenic, MQL and nano-coolant machining environment in turning of Inconel 718. Ind Lubr Tribol. 2025;77(2):215-228. https://doi.org/10.1108/ILT-09-2024-0322
[41] Haq MAU, Hussain S, Ahmad S, Khan AM, Pimenov DY, Giasin K. Evaluating the effects of nano-fluids based MQL milling of IN718 associated to sustainable productions. J Clean Prod. 2021;310:127463. https://doi.org/10.1016/j.jclepro.2021.127463
[42] Mughal K, Ali B, Imran M, Khan AM, Sharma S, Li C, et al. Using Nano-Fluids Minimum Quantity Lubrication (NF-MQL) to Improve Tool Wear Characteristics for Efficient Machining of CFRP/Ti6Al4V Aeronautical Structural Composite. Processes (Basel). 2023;11(5):1540. https://doi.org/10.3390/pr11051540
[43] Komanduri R, Hou ZB. Thermal modeling of the metal cutting process—Part II: temperature rise distribution due to frictional heat source at the tool–chip interface. Int J Mech Sci. 2001;43(1):57-88. https://doi.org/10.1016/S0020-7403(99)00104-6
[44] Madan R, Bhowmick S. Fabrication, microstructural characterization and finite element analysis of functionally graded Al-Al2O3 disk using powder metallurgy technique. Mater Today Commun. 2022;32:103878. https://doi.org/10.1016/j.mtcomm.2022.103878
[45] Madan R, Bhowmick S, Saha K. A study based on stress-strain transfer ratio calculation using Halpin-Tsai and MROM material model for limit elastic analysis of metal matrix FG rotating disk. FME Trans. 2020;48(1):204-210. https://doi.org/10.5937/fme2001204M